

Half-metallic compositional ranges for selected Heusler alloys

Nikolai A. Zarkevich,^{1,*} Prashant Singh,¹ A. V. Smirnov,¹ and Duane D. Johnson^{1,2,†}

¹*Ames Laboratory, U.S. Department of Energy, Ames, Iowa 50011 USA*

²*Departments of Materials Science & Engineering, Iowa State University, Ames, Iowa 50011 USA*

(Dated: April 15, 2020)

For a material that is a half-metal, there should exist a range of compositions for half-metallicity. This compositional range can be expressed in terms of *electron count* and computed. We investigate electronic and magnetic properties of doped full- and half-Heusler alloys (stoichiometry XYZ_2 and XYZ , respectively) with elements X from groups 13–16 and periods 3–6 of the Periodic Table, $Y=\{\text{Mn, Fe}\}$, and $Z=\{\text{Co, Ni}\}$. Using spin density functional theory, we predict shifts of the Fermi energy in the doped and solid-solution alloys. These predictions can be used for band-gap engineering of multicomponent half-metals and provide the viable range of compositions, such as for a range of $n = x + y + z$ in $(\text{Co}_{2-z}\text{Ni}_z)(\text{Mn}_{1-y}\text{Fe}_y)(\text{Sn}_{1-x}\text{Sb}_x)$. This methodology for doped and chemically disordered half-metallic alloys offers a design approach to electronic-structure engineering that can accelerate development of half-metals for novel electronic and spintronic applications.

Keywords: half-metallicity, band structure, electronic structure engineering, Heusler alloys, magnets.

I. INTRODUCTION

Materials discovery for alloys with specific properties, particularly for viable concentration ranges for half-metallicity, is greatly accelerated by theoretical guidance [1–8], especially in the electronic-structure engineering of doped or chemically disordered alloys. The associated compositional (and electron count) change alters electronic, magnetic, and other (including surface [9]) physical properties [10–13]. Here we study the electronic structure and its dependence on composition in fully and partially-ordered Heusler alloys, some of which are half-metallic. Our results provide valuable guidance for adjusting the width and position of band gaps in the minority spins relative to the Fermi energy, E_F .

Heusler alloys [14] are a large class of naturally occurring [15] and manufactured [16] ternary intermetallic compounds with $L2_1$ full Heusler (fH) or $C1_b$ half-Heusler (hH) structure, which can be partially disordered [17–25]. The known competing structures are the inverse Heusler and hexagonal $D0_{19}$ [26, 27]. Many Heuslers are ferromagnetic (FM), with Curie temperatures T_c between 200 and 1100 K [28–30]. The ones with T_c near room temperature were considered for magnetocalorics [1, 31]. Some alloys have a band gap in the minority spins, which may (as in half-metals [10, 32–41]) or may not be at E_F .

A half-metal conducts electrons with one spin orientation, but acts as an insulator or semiconductor (with a band gap at E_F) for electrons of opposite spins. Half-metals are used in small-scale magnetic and spin filtering devices [42–44] and switches [45], and find applications in magnetic materials [46]. The band-gap engineering [47, 48] helps to create materials for advanced electronic devices. Such solid-state devices are used in spintronics – a rapidly developing branch of electronics, incorporating electron spin degree of freedom (DoF) [49, 50].

We focus on the electronic properties of doped fH- $Z_2\text{MnX}$ and hH- $Z\text{MnX}$ alloys, with $Z=\{\text{Co, Ni}\}$ and $X=\{\text{Al, Ga, In, Tl; Si, Ge, Sn, Pb; P, As, Sb, Bi; S,$

$\text{Se, Te}\}$, elements from groups 13–16 and periods 3–6 in the Periodic Table [51]. We compute the electronic structure of these alloys and predict compositional intervals for half-metallicity in terms of electron count n . We extend compositions to address Mn alloyed with Fe in $\text{Co}_2(\text{Mn}_{1-y}\text{Fe}_y)\text{A}$, where A is Sn or Sb, and $0 \leq y \leq 1$.

We find that in fH- Co_2MnX the width of the minority-spin band gap E_{gap} decreases with period (3–6) and increases with group (13–16) of X. Most of these alloys are stable. Due to small mixing enthalpies, they allow substitutional disorder on each sublattice at room temperature T . For the hH- NiMnX alloys considered, the gap in the minority-spin manifold lies at or slightly above E_F . Five of them (with $X=\text{Si, Ge; P, As, Sb}$) could be half-metals, but only NiMnSb is stable. The structural stability restricts design of hH half-metals.

Often half-metals have lower formation energies (hence are more stable) than their metal counterpart. Interestingly, we predict a possible existence of weakly stable multicomponent half-metallic bismuthides. Considering a doped hH- NiMnBi , we predict that adding from 0.3 to 1.3 electrons per formula unit ($e^-/\text{f.u.}$) would turn this compound into a half-metal. We confirm this prediction for the quaternary $\text{CuNi}_3\text{Mn}_4\text{Bi}_4$ and $\text{ZnNi}_7\text{Mn}_8\text{Bi}_8$ alloys. We analyze stability by considering relative structural energies and cross-sections of the ground-state formation energies versus composition (sometime referred to as the ground-state hull).

This paper is organized by Section II specifying the crystal structures and compositional ranges, Section III identifying computational methods, Section IV containing results and discussion, followed by a summary in Section V. Technical details are provided in Appendix A. Metallic fH- Ni_2MnX is considered in Appendix B.

II. STRUCTURES AND COMPOSITIONS

Crystal Structure: The full-Heusler and half-Heusler

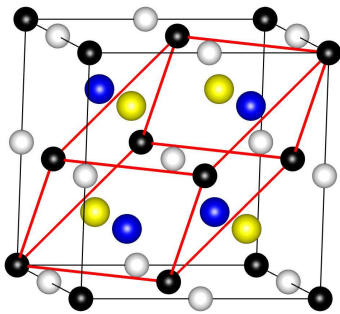


FIG. 1. Heusler $MM'YX$ structure [$F\bar{4}3m$, space group #216] has atoms on bcc sites, denoted as M (black), M' (white), $Y=\{\text{Mn, Fe}\}$ (blue), and X (yellow). Conventional (black) and primitive (red) unit cells are outlined. $C1_b$, cF12 hH-MYX has vacant M' ($\frac{1}{2}, \frac{1}{2}, \frac{1}{2}$) sites. $L2_1$, cF16 ($Fm\bar{3}m$, #225) fH-Z₂YX has Z on both M and M' sites. Inverse Heusler has the same atoms on M and X sites, but M and M' differ.

alloys crystallize in $L2_1$ and $C1_b$ structures, respectively. Fig. 1 represents the quaternary LiMgPdSn-type Heusler, Cu_2MnAl -type fH, AgAsMg -type hH, and the inverse-Heusler structures; caption provides the space group, etc. The fH-Z₂YX ($L2_1$, cF16) structure with Cu_2MnAl prototype has a 16-site conventional cubic unit cell with 3 atom types (decorating a body-centered cubic (bcc) lattice), consisting of four interpenetrating fcc sublattices with positions (0,0,0) and ($\frac{1}{2}, \frac{1}{2}, \frac{1}{2}$) for Z, ($\frac{1}{4}, \frac{1}{4}, \frac{1}{4}$) for Y (Mn) and ($\frac{3}{4}, \frac{3}{4}, \frac{3}{4}$) for X atoms. The primitive unit cell has only 4 sites (outlined in red in Fig. 1). The hH-M₁YX ($C1_b$, cF12) structure with MgAgAs prototype differs from cF16 fH by a vacancy on ($\frac{1}{2}, \frac{1}{2}, \frac{1}{2}$) sites.

Compositions: We consider fH-Z₂YX and hH-M₁YX systems with $Z=\{\text{Co, Ni}\}$; $M=\{\text{Ni}\}$; $Y=\{\text{Mn}\}$; and $X=\{\text{Al, Ga, In, Tl; Si, Ge, Sn, Pb; P, As, Sb, Bi; S, Se, Te}\}$, as well as solid-solution $\text{Co}_2(\text{Mn}_{1-x}\text{Fe}_x)\text{A}$ with $A=\{\text{Sn or Sb}\}$. Our investigation covers both fully-ordered and partially-disordered (substitutional) alloys.

III. SYNOPSIS OF METHODS

A. Guidance for materials engineering

Electron count \mathcal{E} composition: Historically, the search for half-metals started from line compounds [28, 52–54]. We emphasize that E_F remains in the band gap within a range of energies, bounded by the highest occupied and the lowest unoccupied states in the minority spins, and there is a corresponding range of half-metallic compositions.

Indeed, the number of valence electrons $N(c)$ depends on composition c . In Figure 2 we illustrate the inverse [many-to-one $c(N)$] relation for the ternary Ni-Mn-X alloys. A fixed N specifies a set of compositions, leaving sufficient freedom in choosing elements for doping. For example, hH alloys with compositions

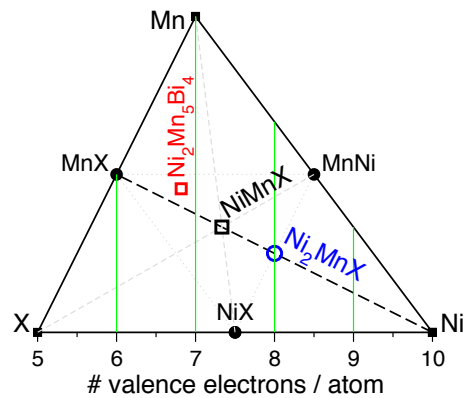


FIG. 2. Isosurfaces of electron count per atom (vertical lines) for Ni-Mn-X with elements $X = \{\text{P, As, Sb, Bi}\}$.

$\text{NiMn}(\text{P}_x\text{As}_y\text{Sb}_z\text{Bi}_w)$, where $0 \leq \{x, y, z, w\} \leq 1$ and $x + y + z + w = 1$, have $N = 7\frac{1}{3}$, see Fig. 2. Below we express the electron count n as a difference in the number of valence electrons relative to a line compound.

Half-metallic range: In each compound, we find a band gap in the minority spins (if any) of the width $E_{\text{gap}} = (E_+ - E_-)$ at the electronic energies E in the range $E_- \leq (E - E_F) \leq E_+$. A compound is half-metallic, if E_F happens to be in this gap (thus, $E_- < 0$ and $E_+ > 0$).

The number of electronic states below E_0 is

$$N(E_0) = \int_{-\infty}^{E_0} dE g(E), \quad (1)$$

where $g \geq 0$ is the electronic density of states (DOS) for both spins. At zero electronic temperature, all states below the E_F are filled, hence $N(E_F)$ is equal to the total number of electrons N . (If one uses pseudopotentials or does not count core electrons, then one can use the total number of valence electrons.) A band gap in the minority spins covers a range of both occupied and empty states from $N_- \equiv N(E_F + E_-)$ to $N_+ \equiv N(E_F + E_+)$; those are the edges of the band gap. Next, we use eq. 1 to find the differences

$$n_{\pm} \equiv (N_{\pm} - N) = \int_{E_F}^{E_F + E_{\pm}} g(E) dE. \quad (2)$$

A compound is half-metallic, if $n_- < 0$ and $n_+ > 0$, see Tables I and II.

Within the frozen-band approximation, let us increase the total number of electrons from N to $(N + n)$; negative n stands for subtracting electrons. The added or subtracted electrons will shift E_F to the band gap (thus making the system half-metallic), if

$$n_- \leq n \leq n_+. \quad (3)$$

In general, doping a conductor with electronic donors or acceptors changes the number of electrons, shifts E_F , and adds impurity states. If those impurity states are

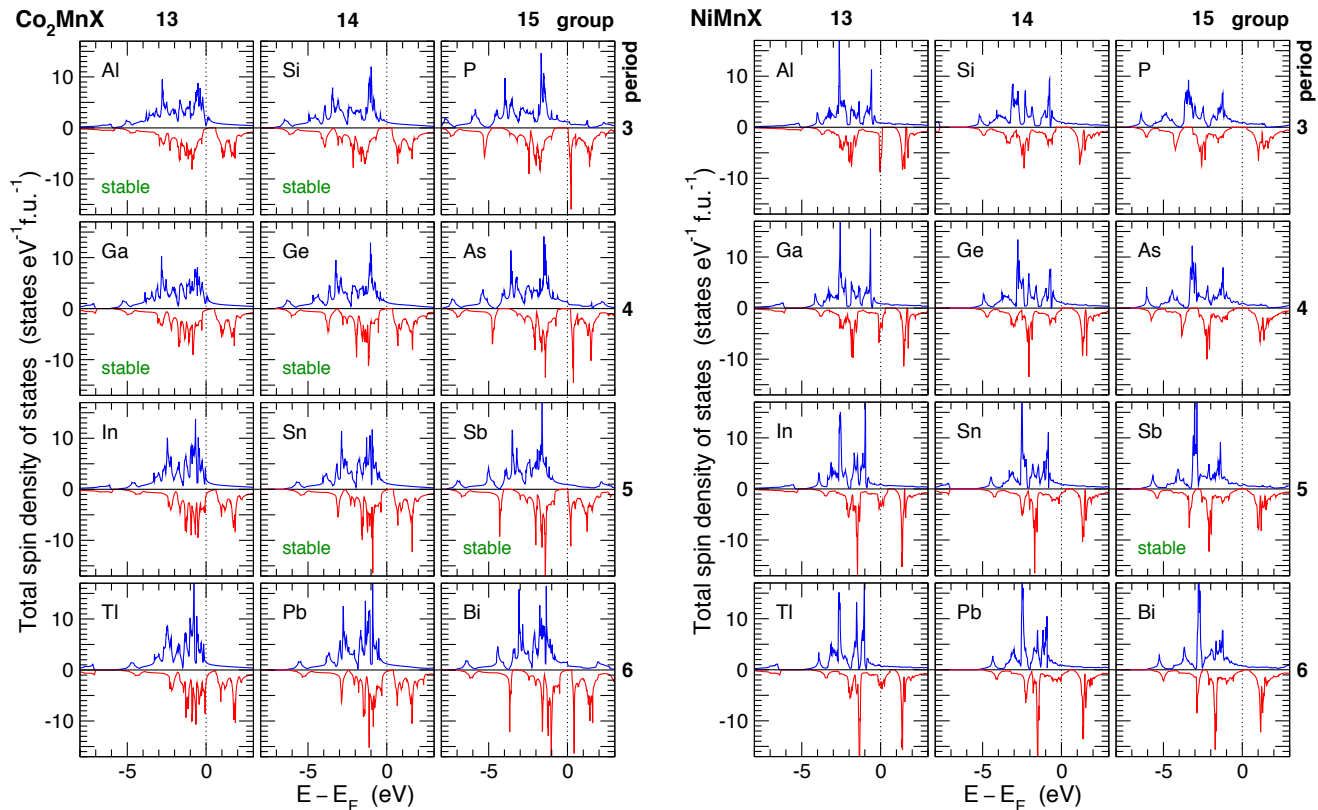


FIG. 3. Electronic spin DOS (states/eV·f.u.) for fH-Co₂MnX (left) and hH-NiMnX (right) for 12 elements X (group 13-15, period 3-6). Stable compounds are known from experiment [28, 29, 55].

not in the band gap, then half-metallicity of the doped system is approximated by inequality (3).

Lattice relaxations around impurities and defects broaden the bands and narrow the band gap. In addition, sometimes electronic bands of the dopant can appear in the band gap. These effects narrow both the band gap and the half-metallic compositional range. With this caution, inequality (3) and Tables I and II provide a practical guidance for engineering of the advanced half-metals.

B. Computational Methods

DFT codes: We calculate energetics and electronic structure using density functional theory (DFT). To verify accuracy of the predicted structural energies and electronic bands in ordered and disordered alloys, we use three DFT codes: a pseudo-potential plane-wave code implemented in VASP [56, 57], an all-electron KKR-CPA Green's Function code MECCA [58], and a TB-LMTO-vLB code with a locally corrected exchange potential [59] that yields bandgaps comparable to hybrid exact-exchange and GW methods [60–62], but with the speed of local density approximation, see Appendix A for details (k -mesh grids, exchange-correlation, etc.).

Structural stability: To address stability, we calculate for each structure the formation energies versus compo-

sition. Each structure on the ground-state (GS) hull is stable and has a nonpositive (negative or zero) formation energy. Structures with energies above the GS hull are either unstable or metastable. They might be stabilized by entropy at finite temperature T ; they can transform or segregate with energy release at lower T .

Accuracy of bandgap widths: The calculated band gap in each spin channel depends on the exchange-correlation functional. Both local density approximation (LDA) and generalized gradient approximation (GGA) usually underestimate the band gap in semiconductors and half-metals; this systematic error narrows the predicted compositional range for half-metals. An error in the predicted band gaps is larger in LDA, smaller in GGA [63], and is expected to cancel for the exact exchange and correlation. Hence, we check results in Tables I and II using a spin-polarized version of van Leeuwen and Baerends (vLB) correction to LDA; with speed of local functionals, this LDA+vLB approximation for exact exchange reproduces hybrid-exchange bandgaps [59–61].

IV. RESULTS AND DISCUSSION

Known half-metals among ternary systems include full Heusler Co₂MnX with X={Si, Ge, Sb} [64, 65] and half-Heusler NiMnSb compounds [66]. However, spin polar-

ization depends on composition, ordering [67, 68], and temperature [69]. We emphasize that not only the line compounds, but also ranges of compositions (with off-stoichiometric disorder) can be half-metallic. We compute the compositional ranges that keep known half-metals half-metallic, and predict the level of doping that can turn others (like Co_2MnSn and hypothetical NiMnBi) into half-metals.

A. Data for electronic-structure engineering

Electronic DOS: We compare the calculated electronic DOS for the ternary line compounds Co_2MnX and Ni_1MnX in Fig. 3. We use experimental data to mark the known stable compounds. The values of E_{\pm} and n_{\pm} , defined in section IIIA, are provided in Tables I and II for fH- Co_2MnX and hH- NiMnX (which have the minority-spin band gap in the vicinity of E_F). This data is useful for engineering materials with a modified electronic structure and for predicting the band gaps in disordered alloys, some of which will be considered in section IV B.

Minority-spin band gaps: Interestingly, we find minority-spin band gaps (or pseudo-gaps) in all ferromagnetic compounds (both stable and unstable), see Fig. 3. In fH Co_2MnX the gaps are at or near E_F . Similarly, in hH NiMnX they are at or slightly above E_F . In contrast, there are no half-metals among fH Ni_2MnX alloys (relegated to Appendix B, see Fig. 14). Because Ni has more electrons than Co, the difference between the fH Co_2MnX and Ni_2MnX is expected from the electron count, explained in section III A. Indeed, the gaps are near E_F in Co_2MnX , but quite far (~ 1 eV) below E_F in Ni_2MnX .

Tables I and II show the band gap $E_{gap} = (E_+ - E_-)$ for the minority spins from GGA (VASP) and LDA+vLB (TB-LMTO) results. The gap extends from E_- to E_+ (both energies are relative to E_F); for half-metals, these are energies of the highest occupied and the lowest un-

occupied bands in the minority spins. The line compound is half-metallic, if $E_- \leq 0$ and $E_+ \geq 0$ (consequently, $n_- \leq 0$ and $n_+ \geq 0$). For half-metals with off-stoichiometric disorder, the level of doping in terms of n (added electrons per formula unit) lies within the range $[n_-, n_+]$. As explained in section III A, dopants narrow the gap, hence the actual compositional range can be narrower. Importantly, our data allows to adjust composition towards E_F in the middle of the gap.

B. Substitutionally Disordered Alloys

In materials engineering, considering multicomponent alloys with a partial disorder can be challenging. Below we analyze quantitatively selected fH alloys, which have three sublattices (Fig. 1), and substitutional alloying is possible on each. We illustrate this with solid-solution fH alloys with disorder on one sublattice and validate predictions, based on the electron count. We consider $\text{Co}_2\text{Mn}(\text{Sn}_x\text{Sb}_{1-x})$, $(\text{Co}_x\text{Ni}_{1-x})_2\text{MnA}$, and $\text{Co}_2(\text{Mn}_{1-x}\text{Fe}_x)\text{A}$ with $\text{A}=\{\text{Sn or Sb}\}$.

We emphasize that disorder on different sublattices can produce a similar shift of E_F . Indeed, the expected similarity of the electronic structure of $\text{Co}_2\text{Mn}(\text{Sn}_x\text{Sb}_{1-x})$ and $\text{Co}_2(\text{Mn}_{1-x}\text{Fe}_x)\text{Sn}$ is verified in Fig. 4. Notably, we find that their mixing enthalpies E_{mix} are small compared to $k_B T_0 = 23.55$ meV (k is Boltzmann's constant) at temperature $T_0 = 273.15$ K, see Figs. 5 and 6.

Solid-solution alloys with a small negative mixing enthalpy ($-kT_0 < E_{mix} \leq 0$) can be uniform at ambient $T \geq T_0$. In contrast, alloys with a small positive mixing enthalpy ($0 < E_{mix} < kT_0$) can develop a compositional fluctuation, which lowers the enthalpy [1]; however, they do not segregate at $T > E_{mix}/k$. We find that $(\text{Co}_x\text{Ni}_{1-x})_2\text{MnA}$ with $\text{A}=\{\text{Sn or Sb}\}$ have small positive E_{mix} , see Fig. 6.

$\text{Co}_2\text{Mn}(\text{Sn}_{1-x}\text{Sb}_x)$: The calculated magnetization of $\text{Co}_2\text{Mn}(\text{Sn}_{1-x}\text{Sb}_x)$ increases with x approximately lin-

TABLE I. The minority-spin band gap width E_{gap} (eV) and position in terms of energies E_{\pm} (relative to E_F) and electron count n_{\pm} in full-Heusler Co_2MnX ternary line compounds. The unstable compounds are marked with an asterisk (*).

X	n_- n_+ (e/f.u.)	E_- E_+ (eV)	E_{gap}^{GGA} (eV)	E_{gap}^{vLB} (eV)
Al	0.07 0.84	0.06 0.62	0.56	0.38
Ga	0.5 0.84	0.24 0.55	0.31	0.23
In*	0.9 1.0	0.54 0.64	0.10	–
Tl*	1.1 1.1	0.63 0.63	0.0	0.0
Si	-0.6 0.35	-0.39 0.34	0.73	0.49
Ge	-0.2 0.4	-0.12 0.38	0.50	0.37
Sn	0.1 0.45	0.09 0.44	0.35	0.37
Pb*	0.35 0.5	0.28 0.43	0.15	0.11
P*	-1.1 0.05	-0.76 0.04	0.80	0.55
As*	-0.6 0.05	-0.43 0.05	0.48	0.44
Sb	-0.5 0.03	-0.51 0.02	0.53	0.38
Bi*	-0.1 0.2	-0.08 0.27	0.35	0.26

TABLE II. The minority-spin band gap E_{gap} and its position in terms of energies E_{\pm} and electron count n_{\pm} in half-Heusler NiMnX compounds. See sections III A and IV A.

X	n_- n_+ (e/f.u.)	E_- E_+ (eV)	E_{gap}^{GGA} (eV)	E_{gap}^{vLB} (eV)
Al*	0.6 1.2	0.10 0.90	0.80	–
Ga*	0.9 1.3	0.30 1.00	0.70	–
In*	1.25 1.5	0.46 0.88	0.40	0.32
Tl*	1.4 1.6	0.60 0.90	0.30	0.27
Si*	-0.37 0.45	-0.35 0.56	0.91	0.8
Ge*	-0.0 0.57	-0.0 0.7	0.70	0.6
Sn*	0.40 0.72	0.28 0.74	0.46	0.43
Pb*	0.65 0.87	0.45 0.79	0.34	0.28
P*	-0.67 0.22	-0.66 0.28	0.93	0.7
As*	-0.37 0.30	-0.38 0.39	0.77	0.6
Sb	-0.17 0.22	-0.27 0.28	0.55	0.45
Bi*	0.06 0.31	0.07 0.47	0.40	0.34

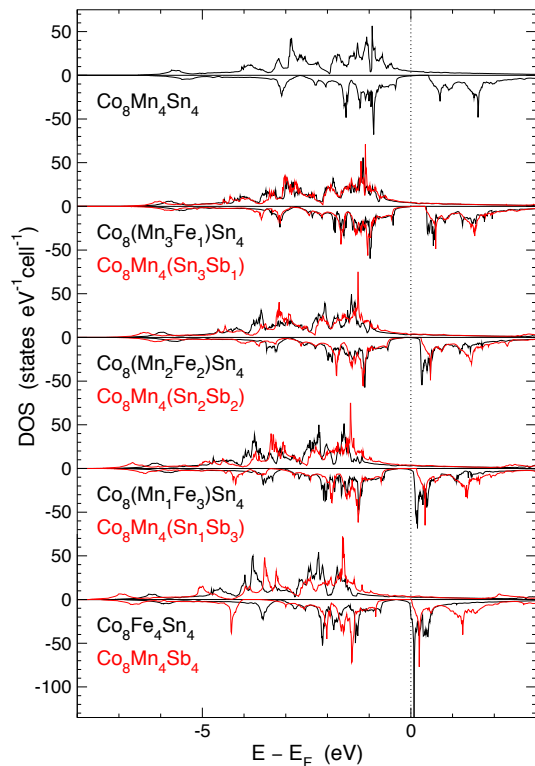


FIG. 4. Total spin-resolved DOS of $\text{Co}_8\text{Mn}_4(\text{Sn}_{4-x}\text{Sb}_{4-4x})$ and $\text{Co}_8(\text{Mn}_{4-4x}\text{Fe}_{4x})\text{Sn}_4$ fully-ordered Heusler with 16-atom cell.

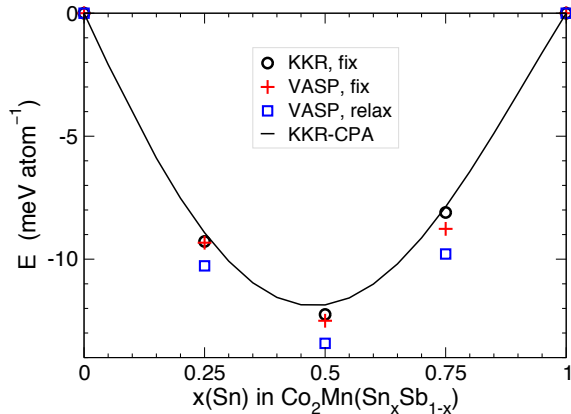


FIG. 5. $\text{Co}_2\text{Mn}_1(\text{Sn}_x\text{Sb}_{1-x})$ mixing enthalpies (meV/atom) at 0 K and 0 Pa. Calculations with fixed atomic coordinates (fix) are compared to those with relaxed atoms (relax). Fully-ordered structures with 16-atom cubic cells are addressed by VASP and KKR; KKR-CPA handles disorder on the (Sn,Sb) sublattice in the 4-atom cell shown in Fig. 1.

early from $1.258 \mu_B/\text{atom}$ in Co_2MnSn to $1.500 \mu_B/\text{atom}$ in half-metallic Co_2MnSb . The equilibrium lattice constants are slightly smaller than those from the Hume-Rothery rule: this indicates the mixing tendency.

Indeed, the trend in mixing enthalpies, calculated for the partially-ordered (KKR-CPA) and fully-ordered

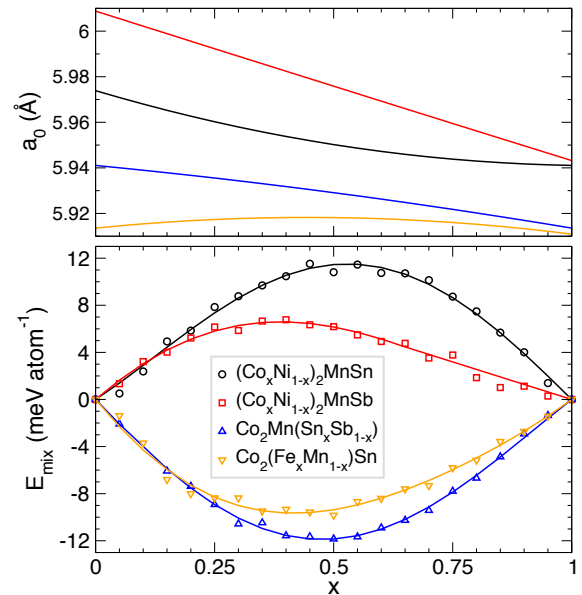


FIG. 6. The equilibrium lattice constants a_0 (Å) and mixing enthalpies E_{mix} (meV/atom) vs. composition x for FH alloys with a homogeneous chemical disorder on one of the sub-lattices obtained using KKR-CPA. Lines are the piece-wise low-degree polynomial fits to DFT data (21 points, symbols).

(VASP and KKR) systems, is the same, see Fig. 5. The predicted stability of disordered $\text{Co}_2\text{Mn}(\text{Sn}_x\text{Sb}_{1-x})$ alloys at room T agrees with experiment [55]. The proposed compositional range of half-metals (given by n in Table I) is confirmed by direct DFT calculations in Fig. 4, which shows that disorder on different sublattices, resulting in the same change of n , can produce similar effects.

Comparing calculations to experiment, we need to take into account that experimental samples are not always precisely stoichiometric. In particular, according to the RBS measurements [55], their Co_2MnSn sample had a Co-excessive composition $\text{Co}_{2.03}\text{Mn}_{1.00}\text{Sn}_{0.97}$, while Co_2MnSb sample was Co-deficient $\text{Co}_{1.98}\text{Mn}_{1.01}\text{Sb}_{1.01}$ ($\text{Co}_{1.94}\text{Mn}_{1.02}\text{Sb}_{1.04}$ according to ICP). Consequently, we expect a slight difference between the equilibrium lattice constants a , calculated for the ideal stoichiometric crystals at 0 K, and measured on the off-stoichiometric samples at finite T . The calculated and experimental [28, 55] lattice constants agree within 1%, see Table III.

$(\text{Co}_{2-x}\text{Ni}_x)\text{MnSb}$: With increasing %Ni, magnetization decreases and a is increasing (Fig. 6). As replacement of Co by Ni in Co_2MnSb moves E_F away from the gap, $(\text{Co}_{2-x}\text{Ni}_x)\text{MnSb}$ are not half-metals at $x > 0.03$, see Table I.

$(\text{Co}_{2-x}\text{Ni}_x)\text{MnSn}$: These alloys can be half-metallic at $0.1 < x < 0.45$, see Table I. The rapidly quenched by melt-spinning $\text{Ni}_{47.3}\text{Mn}_{28.2}\text{Sn}_{24.5}$ sample was confirmed to be half-metallic [70]: this sample has excessive 2.7 at.%Mn replacing Ni and 0.5 at.%Mn replacing Sn.

Figure 7 shows that doping not only shifts E_F , but also narrows the gap. Due to the peak of DOS at the E_F

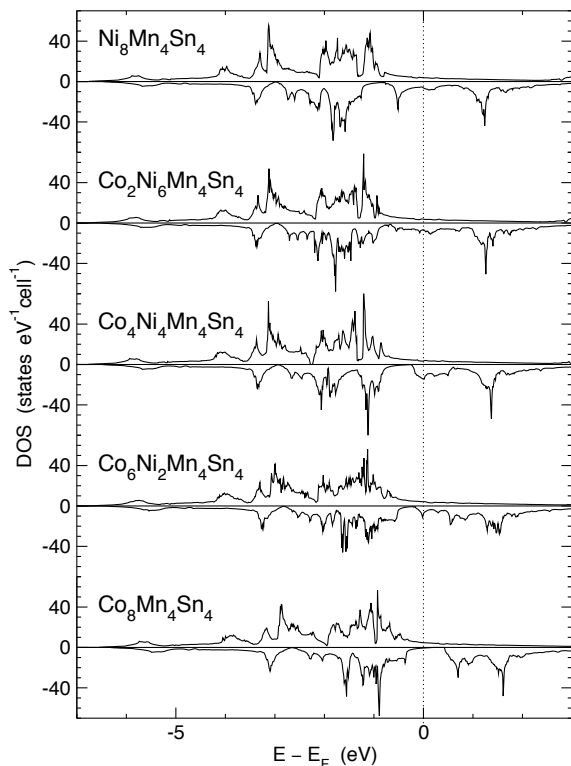


FIG. 7. Total spin DOS (states/eV-f.u.) of $(\text{Co}_{2-x}\text{Ni}_x)\text{MnSn}$ cubic Heusler structures with 16-atom unit cell.

(Fig. 7), cubic CoNiMnSn and $\text{Co}_3\text{NiMn}_2\text{Sn}_2$ structures are unstable. We find that they can be stabilized by a tetragonal distortion, and our findings agree with recent calculations [31].

$\text{Co}_2(\text{Mn}_{1-x}\text{Fe}_x)\text{Sn}$: In Co_2MnSn , the gap in minority spins is located slightly above E_F . Shifting E_F to higher energies should change this alloy into a half-metal, see Fig. 4. Magnetization increases with x from $1.26 \mu_B/\text{atom}$ in Co_2MnSn to $1.41 \mu_B/\text{atom}$ in Co_2FeSn and so does the a (although the atomic radius and magnetic moment of Mn is larger than that of Fe).

$\text{Co}_2(\text{Mn}_{1-x}\text{Fe}_x)\text{Sb}$: In Co_2MnSb the E_F is located at the gap's edge in minority spins (Fig. 3). And, $\text{Co}_2(\text{Mn}_{1-x}\text{Fe}_x)\text{Sb}$ are not half-metals for $x > 0.0$. Replacement of Mn by Fe lowers magnetization from $1.50 \mu_B$ in Co_2MnSb to $1.32 \mu_B/\text{atom}$ in Co_2FeSb , while distortion of $\text{Co}_2(\text{Mn}_{0.5}\text{Fe}_{0.5})\text{Sb}$ from unstable cubic to a more stable tetragonal structure lowers magnetization from 1.42 to $1.23 \mu_B/\text{atom}$. An attempt to mix Mn with Fe on the Mn sublattice quickly moves E_F away from the band gap into the large peak in the minority spin DOS (Fig. 8), making a cubic Heusler structure unstable. Indeed, mixing enthalpies of cubic $\text{Co}_2(\text{Mn}_{1-x}\text{Fe}_x)\text{Sb}$ are positive (relative to the segregated Co_2MnSb and Co_2FeSb), with that for cubic $\text{Co}_2(\text{Mn}_{0.5}\text{Fe}_{0.5})\text{Sb}$ being $+2.1 \text{ meV}/\text{atom}$, while distorted tetragonal $\text{Co}_2(\text{Mn}_{0.5}\text{Fe}_{0.5})\text{Sb}$ has a negative formation enthalpy of $-10.3 \text{ meV}/\text{atom}$.

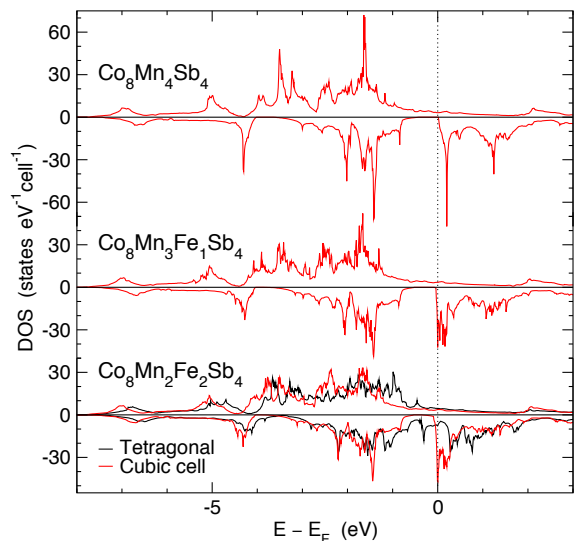


FIG. 8. Total spin DOS (states/eV-f.u.) of $\text{Co}_8(\text{Mn}_{4-4x}\text{Fe}_{4x})\text{Sb}_4$ at $0 \leq x \leq 0.5$ for cubic Heusler (red) and tetragonal (black) 16-atom unit cell.

A similar instability towards tetragonal distortions was predicted for other Co_2 -based Heusler compounds under pressure [71]. We conclude that adding iron to Co_2MnSb can result in formation of other (more stable) compounds with lower magnetization, which are not Heusler.

C. Further Comparison to Experiment

Addressing the ternary line compounds, we fully relaxed each structure (Appendix A 1). We found a reasonable agreement between the calculated and measured

TABLE III. Equilibrium lattice constant a (\AA), magnetic moment M ($\mu_B/\text{f.u.}$), and experimental [28, 29] Curie temperature T_c (K) of fully relaxed fH Co_2MnX alloys from theory (DFT: GGA, see Appendix A 1) and experiment (Expt.). Asterisk (*) marks hypothetical non-existent compounds. Known competing structures include oP12 [72] for $\text{X}=\{\text{Si}, \text{As}\}$ and tI12 [73] for Co_2MnSn .

X	a (\AA)		M ($\mu_B/\text{f.u.}$)		T_c (K)
	DFT	Expt. [28, 29]	DFT	Expt.	Expt.
Al	5.6927	5.749[28], 5.756[29]	4.03	4.04, 4.01	693
Ga	5.7136	5.767[28], 5.770[29]	4.09	4.05, 4.05	694
In*	5.9813	—	4.44	—	—
Tl*	6.0561	—	4.80	—	—
Si	5.6285	5.645[28], 5.654[29]	5.00	4.90, 5.07	985
Ge	5.7358	5.749[28], 5.743[29]	5.00	4.93, 5.11	905
Sn	5.9854	5.984[28], 6.000[29]	5.03	4.79, 5.08	829
Pb*	6.0956	—	5.11	—	—
P*	5.6385	—	6.00	—	—
As*	5.7939	—	5.99	—	—
Sb	6.0182	5.943[55]	6.00	4.52[28]	—
Bi*	6.1793	—	6.00	—	—

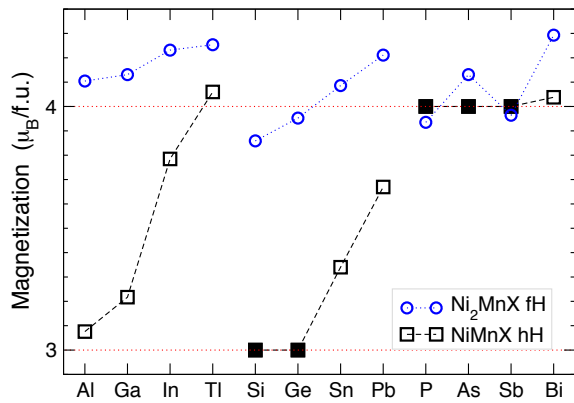


FIG. 9. Calculated magnetization (Bohr magnetons per f.u.) for hH-NiMnX (squares); solid symbols mark half-metals. fH-Ni₂MnX (circles) are ferrimagnetic (see appendix B).

[28, 29] lattice constants a and moments M , see Tables III and IV. We considered both ferromagnetic (FM) and antiferromagnetic (AFM) spin ordering. For the Co₂MnX systems in Fig. 3, we find that FM ordering is preferred, in agreement with the previous calculations [74].

The calculated [56, 57] magnetization M of Co₂MnSn is 5.03 (5.04) μ_B per formula unit with Sn d -electrons in the core (valence) at the equilibrium $a_0 = 5.9854 \text{ \AA}$. It reasonably agrees with the experimental M of 5.08 μ_B . [75] Our all-electron KKR results yield 4.98 μ_B /f.u. at $a_0 = 5.995 \text{ \AA}$, comparing well to earlier FLAPW [76] of 5.0 μ_B /f.u. at $a_0 = 5.964 \text{ \AA}$. However, we note that there is an experimental uncertainty in the weight of the powder sample, only a fraction of which is the desired phase [28]. The imprecisely measured magnetization of the Co₂MnSn and Co₂MnSb polycrystalline powder samples [28] is below the expected theoretical value, which must be integer for a half-metal, and Co₂MnSb is shown to be a half-metal in experiment [28].

D. hH-NiMnX alloys

Among the hH-NiMnX alloys, where X is one of {Al, Ga, In, Tl; Si, Ge, Sn, Pb; P, As, Sb, Bi}, NiMnSb is the only known stable ternary compound, which had been claimed to be a half-metal [32, 77], but its half-metallicity was questioned by some measurements [78] and calculations [79].

We calculate magnetization (Fig. 9), formation energy (Fig. 10), and electronic DOS (Figs. 3 and 14) of hH-NiMnX and fH-Ni₂MnX. Magnetization of the half-metallic hH alloys increases from 3 μ_B /f.u. for NiMnSi and NiMnGe containing group 14 elements to 4 μ_B /f.u. in group 15. An antiferromagnetic (AFM) spin ordering is preferred for most compounds of sulfur, a group 16 element with a small atomic size and high electronegativity.

Among hH alloys, we find five half-metals: they are NiMnX with X={Si, Ge, P, As, Sb}. The first two with

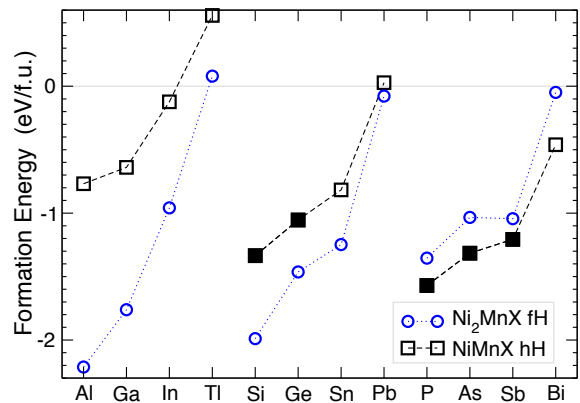


FIG. 10. Formation energy (eV per f.u.) of hH-NiMnX (squares); solid symbols mark half-metals. Results for fH-Ni₂MnX (circles) are given for comparison (see appendix B).

a group 14 element (NiMnSi, NiMnGe) have magnetization of 3 μ_B /f.u., which increases to 4 μ_B /f.u. for the last three (NiMnP, NiMnAs, NiMnSb) with X from group 15. In spite of having large magnetic moments, cubic systems cannot make hard magnets due to absence of anisotropy; a structural anisotropy is necessary for a magnetic anisotropy in a hard magnet.

All considered hH-NiMnX alloys have a gap in the minority spins at or slightly above E_F (Fig. 3 and Table I). In general, a peak with a maximum in the DOS at E_F destabilizes the alloy. Electron (or hole) doping is one option, which shifts E_F away from this peak, and reduces $g(E_F)$. Half-metals are the most stable compounds among the considered hH alloys (Fig. 10).

Figure 11 shows relative energies of the line compounds. The fH-Ni₂MnX alloys with X={As, Bi} are not stable, because their energies are well above the ground-state hull. Although the fH Ni₂MnSb could be stabi-

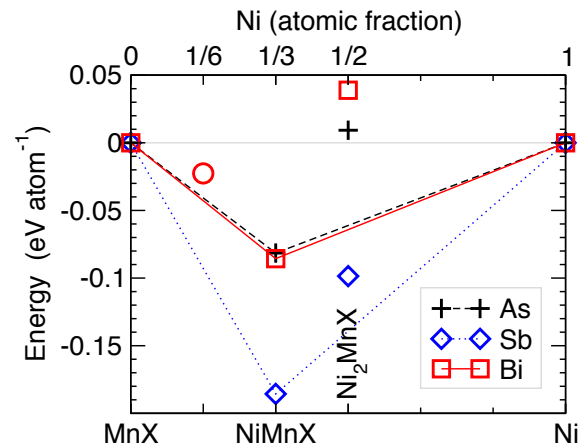


FIG. 11. Energy (eV/atom) of hH-NiMnX relative to fcc Ni and MnX (X = As, Sb, Bi), see Fig. 2, and phase-segregated Ni₂Mn₅Bi₄ and metallic Bi (circle). Ground-state hull is denoted by lines.

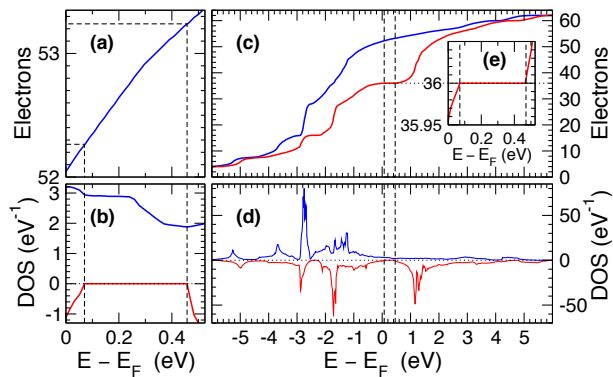


FIG. 12. Number of electrons (per unit cell) and DOS (states/eV·cell) of the hH-NiMnBi.

lized by entropy at finite temperature T , we predict that at low T it tends to segregate towards $\text{Ni}_{2-\delta}\text{MnSb}$ and metallic Ni, although diffusion is limited at low T . The hH-NiMnSb is known to be stable in experiment, and Fig. 11 does not question its stability.

MnNiBi is only $0.06 e^-/\text{f.u.}$ away from being a half-metal; it has a gap in the minority-spin DOS above E_F (Fig. 12), and might be turned into a half-metal by electron doping, such as a partial substitution of Ni by Cu or Zn (Fig. 13). From the estimate of the needed level of doping (see Fig. 12 and Table I), we predict that $\text{CuNi}_3\text{Mn}_4\text{Bi}_4$ and $\text{ZnNi}_7\text{Mn}_8\text{Bi}_8$ should be half-metals. Our supercell calculations (Fig. 13) confirm this prediction, although doping narrows the band gap in the minority spins, as discussed in section III A.

Table II can be used to design half-metals of composition $(\text{Ni}_{1-z-y}\text{Cu}_z\text{Zn}_y)\text{MnX}$ with $X=\{\text{Al, Ga, In, Tl; Si, Ge, Sn, Pb; P, As, Sb, Bi}\}$. For each X , we predicted a range of $n = (z + 2y)$, at which this doped half-Heusler alloy is half-metallic. For negative n , Ni can be mixed with Co and Fe to make $(\text{Ni}_{1-z-y}\text{Co}_z\text{Fe}_y)\text{MnX}$ alloys, where $(z + 2y) = |n| > 0$. Dopants narrow the band gap,

TABLE IV. Lattice constant a (Å) of fully relaxed hH NiMnX alloys from theory (VASP-GGA) and experiment [28, 80, 81]. Other observed competing structures are listed in the last column.

X	NiMnX GGA	hH Expt.	Other Expt.
Al	5.6078	-	
Ga	5.6182		
In	5.9521		
Tl	6.0449		
Si	5.44837		oP12 [72]
Ge	5.570348		oP12, hP6
Sn	5.8903	-	
Pb	6.0412		
P	5.46467		oP12, hP9
As	5.637066		oP12, hP9
Sb	5.9068	5.920 [28]	NiMnSb ₂ hP4
Bi	6.08546		[cF88]

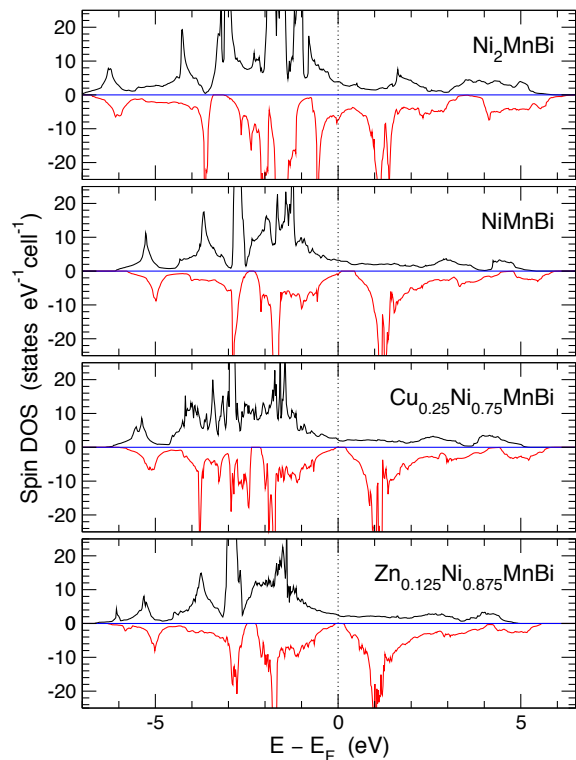


FIG. 13. Total spin DOS (states/eV·f.u.) of hH- Ni_2MnBi (unstable), hH-NiMnBi, and doped hH alloys with substituted N, which shifts E_F and narrows the gap in minority spins.

hence the actual composition range could be narrower than that predicted from electron count.

E. Stability

In general, half-metals are more stable than other metallic half-Heusler alloys, see Fig. 10. We emphasize that a negative formation energy (Fig. 10) relative to the elemental ground states does not necessarily indicate stability of a given phase, because there could be other (more stable) phases nearby, such as the weakly stable $\text{Ni}_2\text{Mn}_5\text{Bi}_4$, NiBi and MnBi in Ni-Mn-Bi system (Fig. 2 and Table V). Energies of all possible competing structures are needed for constructing the complete ground-state hull. While an alloy with a negative for-

TABLE V. Formation energies (eV/atom) of weakly stable bismuth compounds from theory and experiment.

	E (Theory) eV/atom	E (Expt.) eV/atom
MnBi	-0.102	-0.102
NiBi	-0.064	-0.020
$\text{Ni}_2\text{Mn}_5\text{Bi}_4$	-0.117	stable
$\text{CuNi}_3\text{Mn}_4\text{Bi}_4$	-0.106	—
$\text{ZnNi}_7\text{Mn}_8\text{Bi}_8$	-0.115	—

mation energy might be stable, a positive energy relative to any set of phases indicates that a structure is above the ground-state hull and is definitely unstable towards segregation at low T . However, some of the metastable structures are technologically feasible, especially if the phase transformation or segregation has high enthalpy barriers or a metastable phase is thermally stabilized by entropy; examples are iron steels [82–84], Alnico magnets [85], titanium alloys [86], shape memory alloys [87–89], and graphite [90].

F. Predicted Weakly Stable Bismuthides

The ferrimagnetic hexagonal MnBi, NiBi, and magnetic cubic Ni₂Mn₅Bi₄ are weakly stable compounds. In particular, determined from the measured heat of combustion [91] formation enthalpy of MnBi is only -4.7 ± 0.1 kcal/g-formula (-0.102 ± 0.002 eV/atom). The measured formation enthalpy of NiBi is approximately -0.93 kcal/g-formula (-0.020 eV/atom); this value was inaccurate due to inhomogeneity of the sample [92]. The calculated formation enthalpies of NiBi and Ni₂Mn₅Bi₄ reasonably agree with experiment (Table V). Interestingly, we predict a new family of weakly stable half-metallic bismuthides. We look forward towards production of the doped multicomponent half-metals, constructed using electron count in Tables I, II and VI.

V. SUMMARY

If a material is a half-metal, then there exists a range of half-metallic compositions, which can be expressed in terms of the electron count. Within that compositional range, the Fermi energy remains within the band gap in one of the spin manifolds. To offer a guidance for the band-gap engineering, we predict half-metallic compositional ranges for the considered full- and half-Heusler alloys. The key take away is that this is a general methodology to tune materials to a nearby gap.

We addressed both electronic properties and structural stability in a wide class of full- and half-Heusler compounds. We found that many of the Heusler Co₂MnX alloys (with X={Al, Si, Ga, Ge, Sn, Sb}) are stable, have low mixing enthalpies for disorder on each of 3 sublattices, and have a band gap in the minority spins at or near the Fermi energy. Within the predicted compositional ranges, these materials are half-metals. Consid-

TABLE VI. For selected compounds, $[n_-, n_+]$ range (e^- /f.u.), E_- , E_+ , and $E_{gap} = E_+ - E_-$ (eV) from the supercell calculations, see Table I caption.

	n_-	n_+	E_-	E_+	E_{gap}^{GGA}	E_{gap}^{vLB}
NiMnBi	0.06	0.31	0.07	0.47	0.40	0.34
CuNi ₃ Mn ₄ Bi ₄	-0.57	1.1	-0.10	0.25	0.35	0.25
ZnNi ₇ Mn ₈ Bi ₈	-0.12	0.2	-0.11	0.19	0.30	—

ering effect of alloying on half-metallicity, we selectively verify electronic properties by direct calculations in supercells. Our results (see Tables I and II and Fig. 3) facilitate design of multicomponent half-metals (including those with off-stoichiometric chemical disorder) with desired width and position of the spin band gap.

Compared to the searches for half-metals among the stoichiometric line compounds [93–100] (which constitute a finite countable set of discrete points in the compositional space), consideration of half-metallic compositional ranges greatly expands the half-metallic compositional space towards a set of continuous compact regions (mathematically, each interval in one dimension or a compact region in multiple dimensions is an infinite uncountable set of points). Properties of half-metals can be continuously tuned within each compositional region.

ACKNOWLEDGMENTS

This work is supported by the U.S. Department of Energy (DOE), Office of Science, Basic Energy Sciences, Materials Science and Engineering Division. The research is performed at the Ames Laboratory, which is operated for the U.S. DOE by Iowa State University under contract DE-AC02-07CH11358.

Appendix A: Technical details

1. VASP

We use VASP [56, 57] with the projector augmented waves (PAW) [101, 102] and Perdew-Wang (PW91) exchange-correlation functional [103] with Vosko-Wilk-Nusair spin-polarization [104]. We use a dense Γ -centered mesh [105] with at least 72 k -points per \AA^{-1} for the Brillouin zone integration. The tetrahedron method with Blöchl corrections [106] is used to calculate electronic density of states (DOS), while Gaussian smearing with $\sigma = 0.05$ eV is used within the conjugate gradient algorithm for the full structural relaxation at zero pressure.

We calculate structural energies using either primitive unit cells for ternary line compounds or supercells for the multicomponent alloys. For example, CuNi₃Mn₄Bi₄ is considered in a 12-atom hH conventional unit cell, while ZnNi₇Mn₈Bi₈ is addressed in a 24-atom $6.141 \times 6.141 \times 12.305$ \AA supercell using $12 \times 12 \times 6$ k -point mesh. Co₂Mn₁(Sn _{n} Sb _{$1-n$}) alloys in Fig. 5 are considered using a decorated 16-atom conventional cubic unit cell of the fH structure, shown in Fig. 1.

The width of the band gap is estimated from the plateau in the total number of the minority-spin electrons $n_s(E)$, see Fig. 12 (c, e). Counting electrons in the majority-spin channel, we find the number of electrons n_- (n_+), which should be added [$n > 0$] or removed [$n < 0$] to move the highest occupied band (the lowest unoccupied band) in the minority spins to E_F . These num-

bers define the compositional interval of half-metallicity in terms of the electron count.

2. Green's Function KKR-CPA

The Korringa-Kohn-Rostoker (KKR) [107, 108] Green's function code [58] is suitable for both fully ordered and partially disordered multicomponent systems. It treats multiple scattering in the atomic sphere approximation (ASA) [109]. We use the optimal local basis set [58] with the radii of scattering spheres, determined from the atomic charge distributions around each atom and its neighbors. The periodic boundary correction (Voronoi polyhedra) accounts more properly for both electrostatic energy [110] and Coulomb potential. A variational definition [111] of the potential-energy zero (so-called muffin-tin zero) v_0 is used and a proper representation of the topology of charge density in the optimal basis set allows to approach accuracy of the full-potential methods [112].

Our truncated optimal basis set with $l_{\max}=3$ includes s -, p -, d - and f -orbital symmetries; we find a negligible sensitivity of energy differences to the higher-order spherical harmonics. Integration in a complex energy plane uses the Chebyshev quadrature semicircular contour with 20 points. The Brillouin zone integration is performed using a special k -points method [105] with a $12 \times 12 \times 12$ mesh (and a smaller $8 \times 8 \times 8$ supporting grid) for disordered or ordered systems with 4 atoms per unit cell and $8 \times 8 \times 8$ ($6 \times 6 \times 6$) mesh for ordered systems with 16 atoms/cell. Homogeneous, substitutional chemical disorder is considered using the coherent potential approximation (CPA) [113] with the screened-CPA corrections to account for charge-correlations (Friedel screening) associated with local environments [114]. Notably, for homogeneous disorder the unit cell remains the same as for the ternary compounds, due to the mean-field CPA configuration averaging simultaneous with the DFT-based self-consistent-field electronic charge. Hence, we are able to choose any average composition within the same cell, and to continuously adjust the electron count in direct CPA calculations.

For exchange-correlation energies and potentials, we use the generalized gradient approximated (GGA) of Perdew, Burke and Ernzerhof revised for solids (PBEsol) [115]. We perform spin-polarized calculations without spin-orbit coupling. Self-consistency is achieved using the modified Broyden's second method [116].

3. TB-LMTO-vLB

We use the corrected exchange $V_x + V_x^{vLB}$, matched at the ASA radii [59, 117–121], in the exchange-correlation energy parameterization [122] within the local density approximation (LDA). An improved ASA basis of TB-LMTO [123] includes atomic spheres and empty spheres (ESs). The sum of the volumes of all the spheres is equal

the total volume of the periodic unit cell. The radii of the spheres are chosen to have their overlaps close to the local maxima or saddle points of the electrostatic potential. The positions of the ES centers are at the high-symmetry points between atoms. The relaxed atomic positions are taken from VASP output. ESs are treated as empty sites with no cores and small electronic charge density. Because the contribution of exchange in empty spheres is very small, the vLB-correction is calculated only in the atomic spheres [59, 117–121, 124–126]. The core states are treated as atomic-like in a frozen-core approximation. The higher-energy valence states are addressed self-consistently in the effective crystal potential. The last is the muffin-tin potential. The electronic basis combines the plane waves in the nearly free-electron limit outside of the atomic spheres and the spherical harmonics inside the atomic spheres, with the matching imposed at the interfaces [123]. The valence electrons are assumed to be non-relativistic.

Self-consistency is achieved when the change of charge density and energy between iterations becomes small: the relative error for averaged charge density is below 10^{-5} and the absolute error in energies is $< 10^{-4}$ Ry/atom. To facilitate convergence, we use the Anderson mixing. The k -space integration is done using the tetrahedron method with the $12 \times 12 \times 12$ mesh.

In theory, the Coulomb and exchange self-interactions should be cancelled [59, 120, 121]. The LDA and GGA are known to under-estimate band gaps; this problem is less severe in GGA due to the gradient correction [63]. On the other hand, the asymptotic vLB correction significantly improves the exchange potential both near the nucleus ($r \rightarrow 0$) and at the large-distance limit ($1/r \rightarrow 0$). It correctly describes the valence and conduction-band energies, and provides the band gaps comparable to those measured in experiments [59, 120, 121].

4. Formation energy of Mn

To avoid a systematic error in the energy of α -Mn, resulting from application of DFT to an astonishingly complex α -Mn crystal structure with non-collinear moments, we use the semi-empirical energy of metallic Mn, obtained from the calculated energies of metallic Bi [12] and ferrimagnetic MnBi (with NiAs structure) [127], and the experimental [91] formation energy of MnBi of -0.204 eV/f.u. By construction, the calculated formation energy of MnBi coincides with this experimental value.

Appendix B: Metallic fH-Ni₂MnX

We claim that there are no half-metals among the fH Ni₂MnX alloys. We find that the fH Ni₂MnX alloys (with X from groups 13–16 and periods 3–6) are metallic, see Fig. 14. They have high magnetization (Fig. 9); some of them are promising phases for advanced Alnico-type

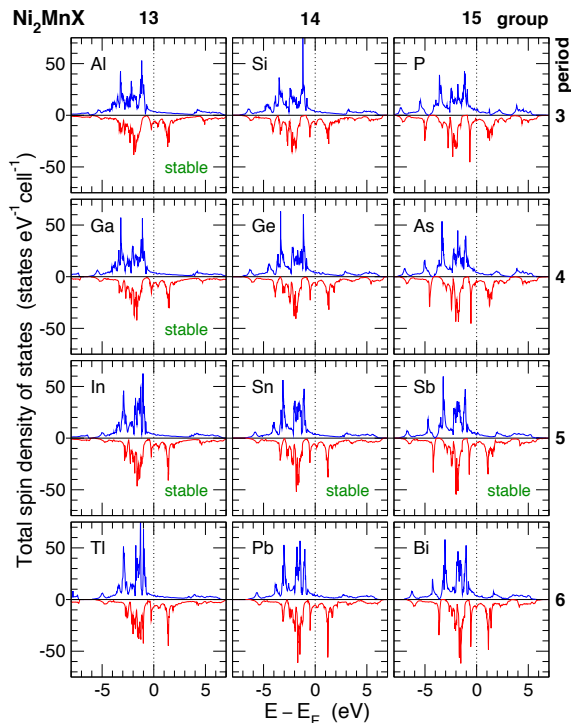


FIG. 14. Total spin DOS (states/eV·f.u.) of fH-Ni₂MnX for 12 elements X from group 13–15 and periods 3–6). All systems are metallic. Compounds that are stable (marked in figure) are known from experiment [80, 81].

magnets, while several might segregate into other compounds (Fig. 11). The electronic-structure calculations reveal a minimum with a small density of the minority spin states, located ≈ 1 eV below the Fermi level, see Fig. 14. We found that there are no half-metals among these alloys, and we do not see a practical way of transforming them into half-metals by a small amount of doping. Thus, we disagree with the suggestion that the rapidly quenched Ni_{47.3}Mn_{28.2}Sn_{24.5} ribbon, prepared by melt-spinning, was half-metallic [70]. We point that although ferromagnets and ferrimagnets can have different conductivity for two spin channels [128], conductivity of half-metals for one of the spins is zero. We find that Ni₂MnSn is magnetic, but not half-metallic.

The fH Ni₂MnX alloys with X={P, As, Sb, Bi; S, Se, Te} are unstable with respect to nickel segregation (see Fig. 11), because they have a positive formation energy relative to the segregated metallic fcc Ni and hH NiMnX.

Mechanical Distortion: We considered anisotropic distortions of the cubic cells, and found that fH alloys (including Ni₂MnSb and Ni₂MnBi) might distort along the 111 axis with energy lowering, but remain unstable with respect to segregation to fcc Ni and a hH alloy.

* zarkev@ameslab.gov

† ddj@ameslab.gov

- ¹ N. A. Zarkevich, D. D. Johnson, and V. K. Pecharsky, *Journal of Physics D: Applied Physics* **51**, 024002 (2018).
- ² D. P. Tabor, L. M. Roch, S. K. Saikin, C. Kreisbeck, D. Sheberla, J. H. Montoya, S. Dwaraknath, M. Aykol, C. Ortiz, H. Tribukait, C. Amador-Bedolla, C. J. Brabec, B. Maruyama, K. A. Persson, and A. Aspuru-Guzik, *Nature Reviews Materials* **3**, 5 (2018).
- ³ P. Gorai, V. Stevanović, and E. S. Toberer, *Nature Reviews Materials* **2**, 17053 (2017).
- ⁴ A. Jain, Y. Shin, and K. A. Persson, *Nature Reviews Materials* **1**, 15004 (2016).
- ⁵ S. V. Kalinin, B. G. Sumpter, and R. K. Archibald, *Nature Materials* **14**, 973 (2015).
- ⁶ G. Hautier, A. Jain, and S. P. Ong, *Journal of Materials Science* **47**, 7317 (2012).
- ⁷ B. Rohr, H. S. Stein, D. Guevarra, Y. Wang, J. A. Haber, M. Aykol, S. K. Suram, and J. M. Gregoire, *Chem. Sci.* **11**, 2696 (2020).
- ⁸ J. J. de Pablo, N. E. Jackson, M. A. Webb, L.-Q. Chen, J. E. Moore, D. Morgan, R. Jacobs, T. Pollock, D. G. Schlom, E. S. Toberer, J. Analytis, I. Dabo, D. M. DeLongchamp, G. A. Fiete, G. M. Grason, G. Hautier, Y. Mo, K. Rajan, E. J. Reed, E. Rodriguez, V. Stevanovic, J. Suntivich, K. Thornton, and J.-C. Zhao, *npj Computational Materials* **5**, 41 (2019).
- ⁹ J. K. Kawasaki, A. Sharan, L. I. M. Johansson, and et al.,

Science Advances **4**, eaar5832 (2018).

- ¹⁰ Galanakis, I. and Dederichs, P. H. and Papanikolaou, N., *Phys. Rev. B* **66**, 174429 (2002).
- ¹¹ K. E. H. M. Hanssen, P. E. Mijnders, L. P. L. M. Rabou, and K. H. J. Buschow, *Phys. Rev. B* **42**, 1533 (1990).
- ¹² N. A. Zarkevich, *Complexity* **11**, 36 (2006).
- ¹³ M. P. Raphael, B. Ravel, Q. Huang, M. A. Willard, S. F. Cheng, B. N. Das, R. M. Stroud, K. M. Bussmann, J. H. Claassen, and V. G. Harris, *Phys. Rev. B* **66**, 104429 (2002).
- ¹⁴ F. Heusler, *Verh. Dtsch. Phys. Ges.* **5**, 219 (1903).
- ¹⁵ E. Uhl, *J. Solid State Chem.* **43**, 354 (1982).
- ¹⁶ C. Felser and A. Hirohata, eds., *Heusler Alloys: Properties, Growth, Applications* (Springer, 2016).
- ¹⁷ B. Weise, B. Dutta, N. Teichert, A. Hütten, T. Hickel, and A. Waske, *Scientific Reports* **8**, 9147 (2018).
- ¹⁸ S. Li, T. Nakatani, K. Masuda, Y. Sakuraba, X. Xu, T. Sasaki, H. Tajiri, Y. Miura, T. Furubayashi, and K. Hono, *Acta Materialia* **142**, 49 (2018).
- ¹⁹ M. N. Guzik, C. Echevarria-Bonet, M. D. Riktor, P. A. Carvalho, A. E. Gunnaes, M. H. Sorby, and B. C. Hauback, *Acta Materialia* **148**, 216 (2018).
- ²⁰ E. Rausch, M. V. Castegnaro, F. Bernardi, M. C. M. Alves, J. Morais, and B. Balke, *Acta Materialia* **115**, 308 (2016).
- ²¹ G. Rogl, A. Grytsiv, M. Gurth, A. Tavassoli, C. Ebner, A. Wunschek, S. Puchegger, V. Soprunyuk, W. Schranz, E. Bauer, H. Muller, M. Zehetbauer, and P. Rogl, *Acta*

- Materialia **107**, 178 (2016).
- ²² M. Gurth, G. Rogl, V. Romaka, A. Grytsiv, E. Bauer, and P. Rogl, *Acta Materialia* **104**, 210 (2016).
- ²³ J. E. Fischer, J. Karel, S. Fabbri, P. Adler, S. Ouardi, G. H. Fecher, F. Albertini, and C. Felser, *Phys. Rev. B* **94**, 024418 (2016).
- ²⁴ M. G. Kostenko, A. V. Lukoyanov, and E. I. Shreder, *JETP Lett.* **107**, 126 (2018).
- ²⁵ S. KC, R. Mahat, S. Regmi, A. Mukherjee, P. Padhan, R. Datta, W. H. Butler, A. Gupta, and P. LeClair, *Phys. Rev. Materials* **3**, 114406 (2019).
- ²⁶ M. Kratochvílová, D. Král, M. Dušek, J. Valenta, R. Colman, O. Heczko, and M. Veis, *Journal of Magnetism and Magnetic Materials* **501**, 166426 (2020).
- ²⁷ S. Keshavarz, N. Naghibolashrafi, M. Jamer, K. Vinson, D. Mazumdar, C. Dennis, W. Ratcliff, J. Borchers, A. Gupta, and P. LeClair, *Journal of Alloys and Compounds* **771**, 793 (2019).
- ²⁸ K. Buschow, P. van Engen, and R. Jongebreur, *Journal of Magnetism and Magnetic Materials* **38**, 1 (1983).
- ²⁹ P. J. Webster, *J. Phys. Chem. Solids* **32**, 1221 (1971).
- ³⁰ P. J. Brown, K. U. Neumann, P. J. Webster, and K. R. A. Ziebeck, *Journal of Physics: Condensed Matter* **12**, 1827 (2000).
- ³¹ A. Grünebohm, H. C. Herper, and P. Entel, *Journal of Physics D: Applied Physics* **49**, 395001 (2016).
- ³² R. A. de Groot, F. M. Mueller, P. G. v. Engen, and K. H. J. Buschow, *Phys. Rev. Lett.* **50**, 2024 (1983).
- ³³ K. E. H. M. Hanssen and P. E. Mijnen, *Phys. Rev. B* **34**, 5009 (1986).
- ³⁴ M. J. Otto, R. A. M. van Woerden, P. J. van der Valk, J. Wijngaard, C. F. van Bruggen, C. Haas, and K. H. J. Buschow, *Journal of Physics: Condensed Matter* **1**, 2341 (1989).
- ³⁵ S. Fujii, S. Ishida, and S. Asano, *Journal of the Physical Society of Japan* **58**, 3657 (1989).
- ³⁶ S. Fujii, S. Sugimura, Ishida, and S. Asano, *Journal of Physics: Condensed Matter* **2**, 8583 (1990).
- ³⁷ S. Fujii, S. Ishida, and S. Asano, *Journal of the Physical Society of Japan* **64**, 185 (1995).
- ³⁸ I. Galanakis, P. H. Dederichs, and N. Papanikolaou, *Phys. Rev. B* **66**, 134428 (2002).
- ³⁹ I. Galanakis, P. Mavropoulos, and P. H. Dederichs, *Journal of Physics D: Applied Physics* **39**, 765 (2006).
- ⁴⁰ K. Nawa and Y. Miura, *RSC Adv.* **9**, 30462 (2019).
- ⁴¹ Q. Gao, I. Opahle, and H. Zhang, *Phys. Rev. Materials* **3**, 024410 (2019).
- ⁴² I. Galanakis and P. Dederichs, eds., *Half-metallic Alloys: Fundamentals and Applications* (Springer, Berlin, Heidelberg, 2005).
- ⁴³ S. Li, K. V. Larionov, Z. I. Popov, T. Watanabe, K. Amemiya, S. Entani, P. V. Avramov, Y. Sakuraba, H. Naramoto, P. B. Sorokin, and S. Sakai, *Advanced Materials* **32**, 1905734 (2020).
- ⁴⁴ A. V. Lukyanenko, A. S. Tarasov, L. V. Shanidze, I. A. Yakovlev, F. V. Zelenov, A. N. Masugin, A. B. Ivanov, F. A. Baron, and N. V. Volkov, *Journal of Physics: Conference Series* **1410**, 012017 (2019).
- ⁴⁵ G.-X. Miao, J. Chang, B.A. Assaf, D. Heiman, and J. S. Moodera, *Nature Comm.* **5**, 3682 (2014).
- ⁴⁶ K. M. Krishnan, *Fundamentals and Applications of Magnetic Materials* (Oxford University Press, 2016).
- ⁴⁷ F. Capasso, *Science* **235**, 172 (1987).
- ⁴⁸ M. Schwarze, W. Tress, B. Beyer, F. Gao, R. Scholz, C. Poelking, K. Ortstein, A. A. Günther, D. Kasemann, D. Andrienko, and K. Leo, *Science* **352**, 1446 (2016).
- ⁴⁹ S. A. Wolf, D. D. Awschalom, R. A. Buhrman, J. M. Daughton, S. von Molnár, M. L. Roukes, A. Y. Chtchelkanova, D. M. Treger, *Science* **294**, 1488 (2001).
- ⁵⁰ C. Felser and G. H. Fecher, ed., *Spintronics: From Materials to Devices* (Springer, New York, 2013).
- ⁵¹ D. I. Mendeleev, *Zhurnal Russkogo Khimicheskogo Obshchestva* **1**, 60 (1869), in Russian.
- ⁵² V. Y. Irkhin and M. I. Katsnelson, *Physics-Uspekhi* **37**, 659 (1994).
- ⁵³ M. Jourdan *et al.*, *Nat. Commun.* **5**, 3974 (2014).
- ⁵⁴ N. I. Kourov, V. V. Marchenkov, K. Belozerova, and H. W. Weber, *J. Exp. Theor. Phys.* **118**, 426s (2014).
- ⁵⁵ M. R. Paudel, C. S. Wolfe, H. Patton, I. Dubenko, N. Ali, J. A. Christodoulides, and S. Stadler, *Journal of Applied Physics* **105**, 013716 (2009).
- ⁵⁶ G. Kresse and J. Hafner, *Phys. Rev. B* **47**, RC558 (1993).
- ⁵⁷ G. Kresse, and J. Hafner, *Phys. Rev. B* **49**, 14251 (1994).
- ⁵⁸ D. D. Johnson, A. V. Smirnov, and S. N. Khan, *MECCA: Multiple-scattering Electronic-structure Calculations for Complex Alloys. KKR-CPA Program, ver. 2.0* (Iowa State University and Ames Laboratory, Ames, 2015).
- ⁵⁹ P. Singh, M. K. Harbola, M. Hemanadhan, A. Mookerjee, and D. D. Johnson, *Phys. Rev. B* **93**, 085204 (2016).
- ⁶⁰ S. Datta, P. Singh, C. B. Chaudhur, D. Jana, M. K. Harbola, D. D. Johnson, and A. Mookerjee, *Journal of Physics: Condensed Matter* **31**, 495502 (2019).
- ⁶¹ B. Sadhukhan, P. Singh, A. Nayak, S. Datta, D. D. Johnson, and A. Mookerjee, *Phys. Rev. B* **96**, 054203 (2017).
- ⁶² S. Datta, P. Singh, D. Jana, C. B. Chaudhur, M. K. Harbola, D. D. Johnson, and A. Mookerjee, *Carbon* (2020), 3.
- ⁶³ J. P. Perdew, *Phys. Lett. A* **165**, 79 (1992).
- ⁶⁴ S. Ahmed, C. Boyer, and M. Niewczas, *Journal of Alloys and Compounds* **781**, 216 (2019).
- ⁶⁵ C. Guillemard, S. Petit-Watelot, L. Pasquier, D. Pierre, J. Ghanbaja, J.-C. Rojas-Sánchez, A. Bataille, J. Rault, P. Le Fèvre, F. Bertran, and S. Andrieu, *Phys. Rev. Applied* **11**, 064009 (2019).
- ⁶⁶ C. Hordequin, D. Ristoiu, L. Ranno, and J. Pierre, *The European Physical Journal B - Condensed Matter and Complex Systems* **16**, 287 (2000).
- ⁶⁷ A. Rajanikanth, Y. K. Takahashi, and K. Hono, *Journal of Applied Physics* **101**, 023901 (2007).
- ⁶⁸ Y. Venkateswara, D. Rani, K. Suresh, and A. Alam, *Journal of Magnetism and Magnetic Materials* **502**, 166536 (2020).
- ⁶⁹ B. Hu, K. Moges, Y. Honda, H.-x. Liu, T. Uemura, M. Yamamoto, J.-i. Inoue, and M. Shirai, *Phys. Rev. B* **94**, 094428 (2016).
- ⁷⁰ M. Nazmunnahar, T. Ryba, J. del Val, M. Ipatov, J. González, V. Hašková, P. Szabó, P. Samuely, J. Kravcak, Z. Vargova, and R. Varga, *Journal of Magnetism and Magnetic Materials* **386**, 98 (2015).
- ⁷¹ M. A. Zagrebin, V. V. Sokolovskiy, and V. D. Buchelnikov, *Journal of Physics D: Applied Physics* **49**, 355004 (2016).
- ⁷² G. A. Landrum, R. Hoffmann, J. Evers, and H. Boysen, *Inorganic Chemistry* **37**, 5754 (1998).
- ⁷³ Matveyeva N.M., Nikitina S.V., and Zezin S.B., *Russ. Metall.* **5**, 132 (1968).
- ⁷⁴ J. Kübler, A. R. William, and C. B. Sommers, *Phys. Rev. B* **28**, 1745 (1983).

- ⁷⁵ P. J. Webster, *Contemporary Physics* **10**, 559 (1969).
- ⁷⁶ S. Picozzi, A. Continenza, and A. J. Freeman, *Phys. Rev. B* **66**, 094421 (2002).
- ⁷⁷ C. Ciccarelli, L. Anderson, V. Tshitoyan, A. J. Ferguson, F. Gerhard, C. Gould, L. W. Molenkamp, J. Gayles, J. Zelezny, L. Smejkal, Z. Yuan, J. Sinova, F. Freimuth, and T. Jungwirth, *Nature Physics* **12**, 855 (2016).
- ⁷⁸ L. Ritchie, G. Xiao, Y. Ji, T. Y. Chen, C. L. Chien, M. Zhang, J. Chen, Z. Liu, G. Wu, and X. X. Zhang, *Phys. Rev. B* **68**, 104430 (2003).
- ⁷⁹ H. Allmaier, L. Chioncel, E. Arrigoni, M. I. Katsnelson, and A. I. Lichtenstein, *Phys. Rev. B* **81**, 054422 (2010).
- ⁸⁰ T. Kanomata, K. Shirakawa, and T. Kaneko, *Journal of Magnetism and Magnetic Materials* **65**, 76 (1987).
- ⁸¹ E. Uhl, *Journal of Solid State Chemistry* **43**, 354 (1982).
- ⁸² K. Bugayev, Y. Bychkov, Y. Konovalov, V. Kovalenko, and E. Tretyakov, *Iron and Steel Production* (MIR, Moscow, 1971).
- ⁸³ N. A. Zarkevich and D. D. Johnson, *Phys. Rev. B* **91**, 174104 (2015).
- ⁸⁴ N. A. Zarkevich and D. D. Johnson, *J. Chem. Phys.* **143**, 064707 (2015).
- ⁸⁵ P. Campbell, *Permanent magnet materials and their applications* (Cambridge University Press, Cambridge, New York, Melbourne, 1994).
- ⁸⁶ N. A. Zarkevich and D. D. Johnson, *Phys. Rev. B* **93**, 020104 (2016).
- ⁸⁷ N. A. Zarkevich and D. D. Johnson, *Phys. Rev. Lett.* **113**, 265701 (2014).
- ⁸⁸ N. A. Zarkevich and D. D. Johnson, *Phys. Rev. B* **90**, 060102 (2014).
- ⁸⁹ N. A. Zarkevich and D. D. Johnson, *J. Chem. Phys.* **142**, 024106 (2015).
- ⁹⁰ F. P. Bundy, *J. Chem. Phys.* **38**, 631 (1963).
- ⁹¹ S. A. Shchukarev, M. P. Morozova, and T. A. Stolyarova, *Zh. Obshch. Khim.* **31**, 1773 (1961), translated: *Russian Journal of General Chemistry* **31** (6), 1657–1660 (1961).
- ⁹² B. Predel, H. Ruge, *Thermochimica Acta* **3**, 411 (1972).
- ⁹³ M. Tas, E. aolu, C. Friedrich, and I. Galanakis, *Journal of Magnetism and Magnetic Materials* **441**, 333 (2017).
- ⁹⁴ A. Amudhavalli, R. Rajeswarapalanichamy, and K. Iyakutti, *Computational Materials Science* **148**, 87 (2018).
- ⁹⁵ M. Babalola and B. Iyorzor, *Journal of Magnetism and Magnetic Materials* **491**, 165560 (2019).
- ⁹⁶ M. A. Sattar, S. A. Ahmad, F. Hussain, and C. Cazorla, *Journal of Materiomics* **5**, 404 (2019).
- ⁹⁷ E. G. Özdemir and Z. Merdan, *Journal of Magnetism and Magnetic Materials* **491**, 165567 (2019).
- ⁹⁸ S. Ghosh and S. Ghosh, *Physica Scripta* **94**, 125001 (2019).
- ⁹⁹ Q. Gao, I. Opahle, and H. Zhang, *Phys. Rev. Materials* **3**, 024410 (2019).
- ¹⁰⁰ T. Aull, E. Şaşıoğlu, I. V. Maznichenko, S. Ostanin, A. Ernst, I. Mertig, and I. Galanakis, *Phys. Rev. Materials* **3**, 124415 (2019).
- ¹⁰¹ P. E. Blöchl, *Phys. Rev. B* **50**, 17953 (1994).
- ¹⁰² G. Kresse, and D. Joubert, *Phys. Rev. B* **59**, 1758 (1999).
- ¹⁰³ J. P. Perdew, J. A. Chevary, S. H. Vosko, K. A. Jackson, M. R. Pederson, D. J. Singh, and C. Fiolhais, *Phys. Rev. B* **46**, 6671 (1992), ERRATUM: *ibid* **48**, 4978 (1993).
- ¹⁰⁴ S. H. Vosko, L. Wilk, and M. Nusair, *Can. J. Phys.* **58**, 1200 (1980).
- ¹⁰⁵ H. J. Monkhorst and J. D. Pack, *Phys. Rev. B* **13**, 5188 (1976).
- ¹⁰⁶ P. E. Blöchl, *Phys. Rev. B* **62**, 6158 (2000).
- ¹⁰⁷ J. Korringa, *Physica* **13**, 392 (1947).
- ¹⁰⁸ W. Kohn and N. Rostoker, *Phys. Rev.* **94**, 1111 (1954).
- ¹⁰⁹ A. Alam and D. D. Johnson, *Phys. Rev. B* **80**, 125123 (2009).
- ¹¹⁰ N. E. Christensen and S. Satpathy, *Phys. Rev. Lett.* **55**, 600 (1985).
- ¹¹¹ A. Alam and D. D. Johnson, *Phys. Rev. B* **85**, 144202 (2012).
- ¹¹² A. Alam, S. N. Khan, A. V. Smirnov, D. M. Nicholson, and D. D. Johnson, *Phys. Rev. B* **90**, 205102 (2014).
- ¹¹³ D. D. Johnson, D. M. Nicholson, F. J. Pinski, B. L. Gyroffly, and G. M. Stocks, *Phys. Rev. Lett.* **56**, 2088 (1986).
- ¹¹⁴ D. D. Johnson and F. J. Pinski, *Phys. Rev. B* **48**, 11553 (1993).
- ¹¹⁵ J. P. Perdew, A. Ruzsinszky, G. I. Csonka, O. A. Vydrov, G. E. Scuseria, L. A. Constantin, X. Zhou, and K. Burke, *Phys. Rev. Lett.* **100**, 136406 (2008).
- ¹¹⁶ D. D. Johnson, *Phys. Rev. B* **38**, 12807 (1988).
- ¹¹⁷ R. van Leeuwen and E. J. Baerends, *Phys. Rev. A* **49**, 2421 (1994).
- ¹¹⁸ P. Singh, M. K. Harbola, B. Sanyal, and A. Mookerjee, *Phys. Rev. B* **87**, 235110 (2013).
- ¹¹⁹ P. Singh, M. K. Harbola, and A. Mookerjee, *Modeling, Characterization, and Production of Nanomaterials*, edited by V. K. Tewary and Y. Zhang (Woodhead Publishing, Massachusetts, 2015) Chap. 16, pp. 407–418.
- ¹²⁰ P. Singh, M. K. Harbola, and D. D. Johnson, *Journal of Physics: Condensed Matter* **29**, 424001 (2017).
- ¹²¹ B. Sadhukhan, P. Singh, A. Nayak, S. Datta, D. D. Johnson, and A. Mookerjee, *Phys. Rev. B* **96**, 054203 (2017).
- ¹²² U. van Barth and L. Hedin, *J. Phys. C: Solid State Phys.* **15**, 1629 (1972).
- ¹²³ O. Jepsen and O. K. Andersen, *The Stuttgart TB-LMTO-ASA program, version 4.7* (Max-Planck-Institut für Festkörperforschung, Stuttgart, Germany, 2000).
- ¹²⁴ M. K. Harbola and V. Sahni, *Phys. Rev. Lett.* **62**, 489 (1989).
- ¹²⁵ V. Sahni and M.K. Harbola, *International Journal of Quantum Chemistry* **38**, 569 (1990).
- ¹²⁶ M. S. M. Hemanadhan and M. K. Harbola, *Journal of Physics B: Atomic, Molecular and Optical Physics* **47**, 115005 (2014).
- ¹²⁷ N. A. Zarkevich, L.-L. Wang, and D. D. Johnson, *APL Materials* **2**, 032103 (2014).
- ¹²⁸ N. A. Zarkevich and D. D. Johnson, *Phys. Rev. B* **97**, 014202 (2018).